Cellular/Molecular

Dopamine Modulates I_h in a Motor Axon

Aleksander W. Ballo,[1] Jennifer C. Keene,[1] Patricia J. Troy,[1] Marie L. Goeritz,[1] Farzan Nadim,[2,3] and Dirk Bucher[1,4]

[1]The Whitney Laboratory for Marine Bioscience, University of Florida, St. Augustine, Florida 32080, [2]Department of Mathematical Sciences, New Jersey Institute of Technology and [3]Department of Biological Sciences, Rutgers University, Newark, New Jersey 07102, and [4]Department of Neuroscience, University of Florida, Gainesville, FL 32611

We studied the axons of the pyloric dilator neurons in the stomatogastric nervous system of the lobster. The several-centimeters-long portions of these axons in the motor nerves depolarize in response to low concentrations of dopamine (DA) and exhibit peripheral spike initiation in the absence of centrally generated activity. This effect is inhibited by blockers of hyperpolarization-activated inward current (I_h). We show here that peripheral spike initiation was also elicited by D_1-type receptor agonists and drugs that increase cAMP. This suggests that DA acts via a D_1-type receptor mechanism to modulate hyperpolarization-activated cyclic nucleotide-gated channels. We used two-electrode voltage clamp of the axon to directly study the effect of DA on I_h. Surprisingly, DA decreased the maximal conductance. However, because of a shift of the activation curve to more depolarized potentials, and a change in the slope, conductance was increased at biologically relevant membrane potentials. These changes were solely caused by modulation of I_h, as DA had no discernible effect when I_h was blocked. In addition, they were not induced by repeated activation and could be mimicked by application of drugs that increase cAMP concentration. DA modulation of I_h persisted in the presence of a protein kinase A inhibitor and is therefore potentially mediated by a phosphorylation-independent direct effect of cAMP on the ion channel. A computer model of the axon showed that the changes in maximal conductance and voltage dependence were not qualitatively affected by space-clamp problems.

Introduction

Axon trunks are increasingly recognized as neuronal compartments with functional roles beyond mere faithful conduction of action potentials (Debanne, 2004; Kress and Mennerick, 2009). Axons often contain a diverse complement of voltage-gated ion channels (Nashmi and Fehlings, 2001; Bean, 2007; Nusser, 2009), with consequences for timing and efficacy of neuronal communication: The different activation and inactivation properties of ion channels can lead to frequency-dependent changes in conduction velocity (Meeks and Mennerick, 2007; De Col et al., 2008; Ballo and Bucher, 2009), spike failures (Miller and Rinzel, 1981; Debanne et al., 1997, 1999; Meeks et al., 2005), or ectopic spike initiation (Kepler and Marder, 1993; Ma and LaMotte, 2007; Jiang et al., 2008), both under normal conditions and as a result of pathological changes (Krishnan et al., 2009).

In addition, the properties of nonsynaptic axonal membrane can be under the control of neuromodulators. Among these are acetylcholine (Lang et al., 2003; Zhang et al., 2004; Kawai et al., 2007), GABA (Sakatani et al., 1991, 1993; Sun and Chiu, 1999; Verdier et al., 2003), and several amines (Meyrand et al., 1992; Mar and Drapeau, 1996; Bucher et al., 2003; Goaillard et al., 2004; Lang et al., 2006; Scuri et al., 2007; Daur et al., 2009). These examples include central and peripheral, unmyelinated and myelinated axons. However, the underlying cellular mechanisms and the potential ion channel targets of axonal modulation are poorly understood, mainly because of the difficulty of obtaining electrophysiological recordings from axons.

We have recently described axonal conduction properties and modulation in an experimentally accessible preparation. In the stomatogastric nervous system (STNS) of the lobster *Homarus americanus*, low concentrations of dopamine (DA) reliably elicit peripheral spike initiation in the two pyloric dilator (PD) axons (Bucher et al., 2003). These axons display complex intrinsic membrane properties that result in activity-dependent changes in resting membrane potential, spike shape, and conduction velocity (Ballo and Bucher, 2009). Both CsCl and ZD7288 (4-ethylphenylamino-1,2-dimethyl-6-methylaminopyrimidinium chloride) block peripheral spike initiation, suggesting that DA predominantly acts by increasing hyperpolarization-activated inward current (I_h) (Ballo and Bucher, 2009). This current, and/or the channels underlying it, are quite commonly found in axons, both in peripheral and central neurons (Nashmi and Fehlings, 2001; Nusser, 2009). It is an inwardly rectifying current activated by hyperpolarization and facilitated by cAMP in a phosphorylation-independent manner (Robinson and Siegelbaum, 2003; Biel et al., 2009; Wahl-Schott and Biel, 2009). This suggests that, in the PD axons, a DA-induced increase in cAMP concentration underlies depolarization and peripheral spike initiation.

We show here that the pharmacological profile of the DA effects on the PD axons is consistent with a D_1-type receptor mechanism increasing cAMP concentration. We also show that

Received Nov. 19, 2009; revised March 9, 2010; accepted March 31, 2010.

This work was supported by National Institute of Neurological Disorders and Stroke Grant NS058825 (D.B.). J.C.K. and P.J.T. were supported by a National Science Foundation (NSF) Research Experiences for Undergraduates site award to The Whitney Laboratory for Marine Bioscience (NSF Grant 0648969). F.N. was supported by National Institute of Mental Health Grant MH60605. We thank Drs. Jorge Golowasch, Peter A. Anderson, and Adam L. Taylor for helpful discussions.

Correspondence should be addressed to Dr. Dirk Bucher, The Whitney Laboratory for Marine Bioscience, University of Florida, 9505 Ocean Shore Boulevard, St. Augustine, FL 32080. E-mail: bucher@whitney.ufl.edu.

M. L. Goeritz's present address: Volen Center for Complex System, Brandeis University, Waltham, MA 02454.

DOI:10.1523/JNEUROSCI.0405-10.2010

 0270-6474/10/308425-10$15.00/0

DA modulates the voltage-dependent activation of I_h in a manner consistent with the observed changes in axonal membrane properties. To our knowledge, this is the first direct demonstration of a neuromodulator affecting the activation properties of a voltage-gated ion channel situated in an axon trunk.

Materials and Methods

Experimental preparation. Adult lobsters (~500 g), *H. americanus*, were obtained from Commercial Lobster and kept in aerated filtered seawater tanks at 10–13°C. Animals were anesthetized on ice before dissection. The STNS was removed from the stomach and placed into a transparent Sylgard-lined (Dow Corning) dish in saline. The saline composition was as follows (in mM): 479.12 NaCl, 12.74 KCl, 13.67 $CaCl_2$, 10 $MgSO_4$, 3.91 Na_2SO_4, and 10 HEPES, pH 7.4–7.5.

Dissections were performed as described previously (Ballo and Bucher, 2009). In short, the stomatogastric ganglion (STG), which contains the somata of the PD neurons, and connected anterior ganglia were kept intact along with the peripheral motor nerves that contain the PD axons innervating the ventral dilator muscles in the intact animal. Both the STG and the unpaired proximal motor nerve leaving the STG, the dorsal ventricular nerve (*dvn*), were desheathed to facilitate drug diffusion and provide access for intracellular recordings. During experiments, preparations were continuously superfused with saline cooled by either custom-made Peltier devices or a SC20/CL-100 cooling system (Warner Instruments). All experiments were performed at 12°C.

Two types of preparations were used. In an initial set of experiments, we obtained extracellular recordings of peripheral spike initiation during drug applications as a pharmacological assay to investigate the DA signaling pathway. Drugs were superfused only to the *dvn* and part of the proximal lateral ventricular nerves (*lvn*), while activity in the STG was pharmacologically blocked and the rest of the preparation was superfused with normal saline. In these experiments, a petroleum jelly well was built around the peripheral nerves and supplied with a separate cooled superfusion system (see Fig. 1*A*). All drug applications were done with continuous superfusion, at rates of ~10 ml/min.

In subsequent experiments, dual intracellular recordings from PD neuron axons were obtained from the *dvn*, and voltage-clamp experiments were performed after different blockers and drugs were bath-applied (see Fig. 3*A*). Recordings were performed at a distance of 5–20 mm to the STG, >3 length constants from the central compartments (Ballo and Bucher, 2009) to ensure that ionic conductances located in central cell compartments did not significantly contribute to the measurements.

Drug applications. Tetrodotoxin (TTX) (100 nM) (Sigma-Aldrich) in saline was bath-applied to block spiking activity in the whole STNS or applied to a petroleum jelly well around the STG to selectively block centrally generated bursting activity. In addition, the following channel blockers were bath-applied in different experiments: 5 mM CsCl (Acros Organics) to block I_h, 4 mM 4-aminopyridine (4-AP) (Sigma-Aldrich) to block transient K^+ currents, and 20 mM tetraethylammonium (TEA) (Fluka) to block delayed rectifier K^+ currents.

3-Hydroxytyramine hydrochloride (DA) (Sigma-Aldrich) was applied at 1 μM. Drugs tested for their potential to interfere with DA signaling included the vertebrate D_1-type receptor agonists chloro-APB hydrobromide (chloro-APB) (20 μM; Sigma-Aldrich) and fenoldopam monohydrobromide (fenoldopam) (20 μM; Sigma-Aldrich), the adenylyl cyclase (AC) activator forskolin (7–10 μM; Sigma-Aldrich), the AC inhibitors 9-(tetrahydro-2-furanyl)-9*H*-purin-6-amine [SQ22,536 (SQ22)] (200 μM; Alexis Biochemicals), *cis*-*N*-(2-phenylcyclopentyl)-azacyclotridec-1-en-2-amine hydrochloride [MDL-12,330A hydrochloride (MDL)] (200 μM; Alexis Biochemicals), 2′,5′-dideoxyadenosine (DDA) (100 μM; Sigma-Aldrich), and 9-cyclopentyladenin monomethanesulfonate (9-CPA) (100 μM; Sigma-Aldrich), the phosphodiesterase (PDE) inhibitor 3-isobutyl-1-methylxanthine (IBMX) (300 μM; Sigma-Aldrich), the cAMP analogs 8-bromoadenosine 3′,5′-cyclic monophosphate (8-br-cAMP) (100 μM; Sigma-Aldrich) and *N*6,2′-*O*-dibutyryladenosine 3′, 5′-cyclic monophosphate (db-cAMP) (1 mM; Sigma-Aldrich), and the protein kinase A (PKA) inhibitor *N*-[2-(*p*-bromocinnamylamino) ethyl]-5- isoquinolinesulfonamide dihydrochloride [H-89 dihydrochloride (H89)] (20 μM; Sigma-Aldrich).

Forskolin and IBMX were dissolved in DMSO before dilution in saline. The final DMSO concentration was 1:1000. We tested that this amount of DMSO alone did not elicit or enhance peripheral spike initiation in the PD axon ($n = 5$).

Electrophysiological recordings. Extracellular recordings of PD spiking activity were obtained by placing a stainless-steel wire electrode into a petroleum jelly well (diameter ≈ 1 mm) built around the distal part of the pyloric dilator nerve (*pdn*). Signals were amplified and filtered using a differential AC amplifier (model 1700; A-M Systems).

As described before (Ballo and Bucher, 2009), intracellular axon recordings required sharp glass microelectrodes. Membrane penetration was achieved by tapping the micromanipulator (Leica) lightly with the back end of dissection forceps. Electrodes were filled with 3 M KCl. Electrode resistances were between 20 and 30 MΩ, and recordings that showed resting membrane potentials more depolarized than −55 mV were discarded. Signals were amplified using an Axoclamp 2B amplifier (Molecular Devices). The lower *dvn* contains some 20 large axons (diameters, ~10 μm). The PD axons were identified by their characteristic waveform during bursts and the correspondence of their spike patterns with the extracellular *pdn* recording. After identification, a second electrode was inserted at a distance of <1 mm. All current measurements were performed in two-electrode voltage-clamp mode.

Data were acquired using a micro 1401 digitizing board and Spike2 software (versions 6 and 7; Cambridge Electronic Design) and analyzed using programs written in the Spike2 script language. Statistical analyses and graphs were generated in SigmaPlot (version 11; Systat) and Statview (version 5; SAS Institute), and final figures in Canvas (version 11; ACD Systems).

Current measurements. I_h was measured using the following protocol: After blocking voltage-gated Na^+ channels with TTX and K^+ currents with TEA and 4-AP, the membrane potential was stepped from a holding potential of −30 mV to a more hyperpolarized potential for 15 s, in increments of 10 mV from −120 to −40 mV in consecutive steps. I_h in STG neurons is a very slowly activating current (Peck et al., 2006). Therefore, no leak subtraction protocol was used, and instead the following method was used for leak subtraction: Single-exponential fits of the current traces were generated in Spike 2, excluding the capacitance artifact at the beginning of the step. The fit was extended in both directions, and I_h was measured as the difference between the steady-state value several seconds after the step and the ("leak") current value at the intersection of the fit and the start of the step. In some experiments, these voltage steps were interleaved with two-part steps to obtain the reversal potential from tail current measurements. To this end, the membrane potential was stepped to −110 mV for 15 s and then immediately to the respective potential of the preceding step (between −120 and −40 mV) for 4 s. The initial leak, measured from the preceding step, was subtracted from the peak of the tail currents. The reversal potential was determined from the zero crossings of linear fits to the *I–V* plots.

From the *I–V* relationship of I_h and the reversal potential, conductances were calculated and fitted with a first-order Boltzman equation of the following form: $g = g_{max}/(1 + e^{-(V_m - V_{half})/s})$, where g is the conductance, g_{max} is the maximal conductance, V_m is the membrane potential, V_{half} is the voltage of half-activation, and s is the slope factor. The activation time constant was determined from a single-exponential fit of the current response to a step from −30 to −110 mV.

Multicompartment modeling of the PD axon. To explore how conductance measurements in the PD axon are affected by space-clamp errors, a realistic computational model of the axon was built that included only passive properties and I_h. The model axon had a diameter of 10 μm and a length of 2.01 cm with sealed ends; the passive parameters used were $R_m = 20$ KΩ cm^2, $R_a = 100$ Ω cm, and $C_m = 1$ μF/cm^2. The resting potential of the axon in the absence of I_h was set to −65 mV. I_h was added in all compartments uniformly as a noninactivating current with first-order activation kinetics. Because the model was only used to measure the value of the current at steady state, the time constant used was unimportant so long as the current reached its steady-state value for each

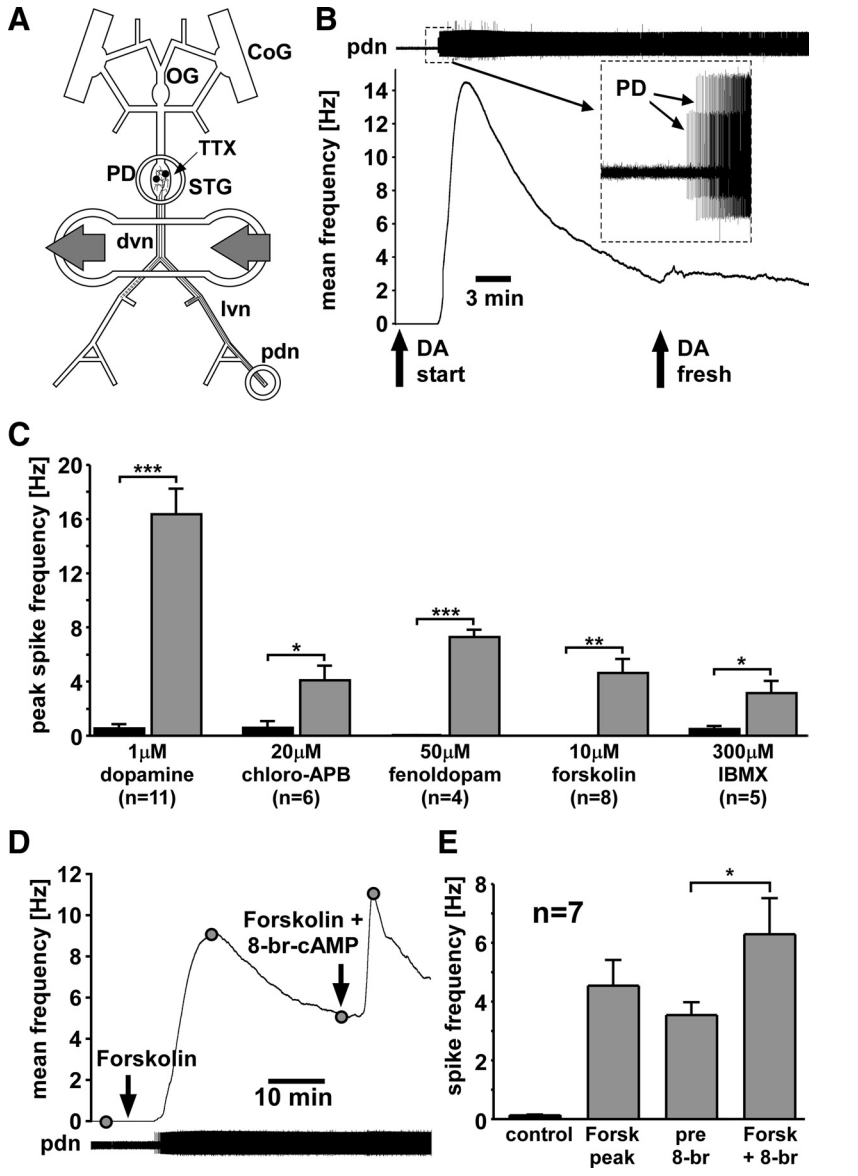

Figure 1. Peripheral spike initiation by DA and drugs that increase cAMP levels. ***A***, Experimental preparation. Centrally generated activity was blocked by application of 100 nM TTX in saline to the STG. Pharmacological agents were applied to a petroleum jelly well built around a part of the *dvn* and proximal *lvns*. Extracellular recordings of PD neuron activity were obtained from a well built around the pdn. CoG, Commissural ganglion; OG, esophageal ganglion. ***B***, PD axon response to application of 1 μM DA. The top trace shows an extracellular record with different amplitude spikes from both PD neurons (inset). Spiking started after DA application. The plot of mean spike frequency over time (bin size, 30 s) shows a fast peak and substantial slow decay of frequency. Spike frequency is not changed by application of fresh DA. ***C***, Peak spike frequencies across experiments compared between control and different drugs. Significance was tested with paired *t* tests. *$p < 0.05$; **$p < 0.01$; ***$p < 0.001$. Error bars are SEM. ***D***, Mean PD axon spike frequency (bin size, 30 s) in response to application of forskolin and subsequent application of forskolin plus 8-br-cAMP. ***E***, Mean spike frequencies in control, peak value in forskolin, and before and after application of forskolin plus 8-br-cAMP. 8-br-cAMP significantly enhanced spiking (paired *t* test).

voltage step. The simulations were therefore done assuming instantaneous activation kinetics. The steady-state activation curve was assumed to be a simple sigmoid $1/(1 + e^{-(Vm - Vhalf)/s})$ with the parameters defined as in the experimental fits described above.

The values of parameters used for I_h were $g_{max} = 7.7 \times 10^{-4}$ S/μm^2, $E_{rev} = -32$ mV in control, and $g_{max} = 4.75 \times 10^{-4}$ S/μm^2, $E_{rev} = -25$ mV in DA. Other parameters are reported in Results. For simulations, the axon was divided into 201 compartments of length 100 μm. The injection electrode was assumed to be in the center, and the recording electrode was set at various distances from the injection electrode as described in Results.

Results

DA acts via a D_1-type signaling pathway, increasing cAMP levels

We used peripheral spike initiation as an assay to pharmacologically determine the DA signaling pathway in the PD axons. We applied DA and other drugs selectively to the peripheral nerves to test which drugs mimic or block the DA effect. Figure 1*B* shows the effect of 1 μM DA applied to the *dvn*/*lvn*. In this experiment, the two PD axons were quiescent in the absence of centrally generated activity before DA was applied. In other experiments, axons displayed spontaneous low-frequency firing or irregular bursting, as described previously (Bucher et al., 2003; Ballo and Bucher, 2009). DA elicited peripheral spike initiation, across experiments peaking after 159 ± 27 s ($n = 11$), as measured from the onset of the response. Spike frequency significantly increased from 0.5 ± 0.3 Hz in control to 16.4 ± 1.9 Hz in DA (paired *t* test, $p < 0.001$) (Fig. 1*C*). After the peak, there was a substantial decrease of frequency over time. This was not attributable to degradation of DA, as frequency continued to decrease when freshly made DA saline was applied (Fig. 1*B*, arrow). The decrease in frequency from the time of the second DA application to 300 s later was significant ($n = 4$; paired *t* test, $p < 0.05$). In some experiments, spike frequency showed a clear single exponential decay with a time constant of several hundred seconds. However, in other experiments, spike frequency was fluctuating substantially while decreasing. We therefore abstained from quantifying this effect.

The D_1-type receptor agonists chloro-APB and fenoldopam both mimicked the DA effect (Fig. 1*C*). Twenty micromolar chloro-APB significantly increased peripheral spiking from 0.6 ± 0.5 to 4.1 ± 1.1 Hz ($n = 6$; paired *t* test, $p < 0.05$). The time to reach peak frequency (415 ± 46 s; $n = 4$) was significantly slower than in DA (unpaired *t* test, $p < 0.001$), and spike frequency, like in DA, decayed substantially within several minutes. Fifty micromolar fenoldopam significantly increased peripheral spiking from 0.04 ± 0.02 to 7.3 ± 0.5 Hz ($n = 4$; paired *t* test, $p < 0.001$). The mean time to reach peak frequency was 434 ± 107 s and therefore also significantly slower than in DA (unpaired *t* test, $p < 0.01$). Spike frequency decayed similarly as in DA and chloro-APB.

Fenoldopam affects dopaminergic regulation of ion transport in crab gills (Genovese et al., 2006), but to our knowledge no information exists in the literature about the specificity of DA receptor agonists in crustaceans. Therefore, we also tested other drugs that potentially affect cAMP signaling. Forskolin, an acti-

vator of AC, and IBMX, an inhibitor of PDE, have been successfully used before to alter cAMP levels in motor axon terminals in *H. americanus* (Goy and Kravitz, 1989). Applied to the PD axons, both drugs mimicked the DA effect (Fig. 1*C*). Ten micromolar forskolin significantly increased spike frequency from 0.02 ± 0.02 to 4.6 ± 1.0 Hz ($n = 8$; paired t test, $p > 0.01$). Three hundred micromolar IBMX significantly increased spike frequency from 0.5 ± 0.2 to 3.1 ± 0.9 Hz ($n = 5$; paired t test, $p < 0.05$). Spike frequency peaked after a significantly longer time in both drugs compared with DA (forskolin: 1696 ± 436 s; unpaired t test, $p < 0.001$; IBMX: 1677 ± 247 s; unpaired t test, $p < 0.001$), and spike frequency markedly decreased after reaching its maximum in both cases.

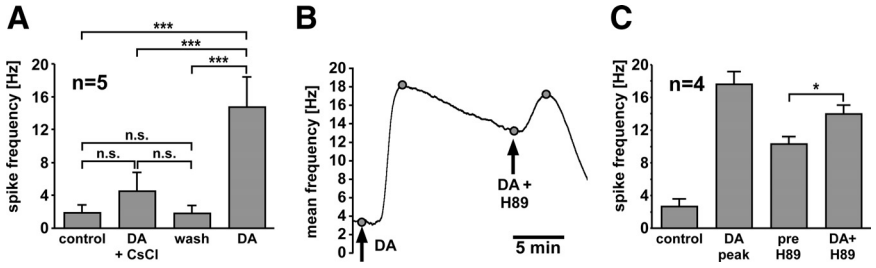

Figure 2. Direct and indirect cAMP pathways. ***A***, Application of DA plus CsCl elicits a significantly smaller spiking response than subsequent application of DA alone (repeated measures ANOVA, Fisher's PLSD *post hoc* comparisons). ***B***, Mean spike frequency (bin size: 30 s) in response to application of DA and subsequent application of DA plus H89. ***C***, Mean values of spike frequencies in control, peak value in DA, and before and after application of DA plus H89. H89 significantly enhanced spiking (paired t test). $^*p < 0.05$; $^{***}p < 0.001$. Error bars are SEM.

The results described above are consistent with an increase in cAMP levels underlying peripheral spike initiation. Surprisingly, direct application of cAMP analogs showed no effect. Neither 1 mM 8-br-cAMP ($n = 3$) nor 1 mM db-cAMP ($n = 2$) increased spike frequency. However, spike frequency increased when we elicited spike initiation with forskolin and then added 8-br-cAMP. Figure 1*D* shows an experiment in which forskolin alone elicited peripheral spike initiation. Twenty minutes after the peak response (after spike frequency had decreased to approximately one-half of the peak value), 8-br-cAMP was applied in conjunction with forskolin, which increased spike frequency substantially. Figure 1*E* shows the mean spike frequency values ($n = 7$) taken at different time points, as indicated in Figure 1*D*. Spike frequency increased significantly from 3.4 ± 0.4 to 6.3 ± 1.2 Hz after application of 8-br-cAMP (paired t test, $p < 0.05$).

In addition, we tested inhibitors of AC that have been used successfully in invertebrates before. MDL and SQ22 inhibit cAMP-dependent activation of a chloride conductance in spiny lobster olfactory receptor neurons (Doolin and Ache, 2005), DDA diminishes serotonergic modulation of cockroach motor neuron responses to acetylcholine (Butt and Pitman, 2002), and 9-CPA disrupts cAMP-dependent expression of motor patterns in the mollusk *Tritonia diomedea* (Clemens et al., 2007). We applied the inhibitors first alone, and then in conjunction with DA. In all cases, DA still elicited peripheral spike initiation, at similar frequencies as the ones shown in Figure 1*C* for DA alone (200 μM MDL, $n = 2$, 21.2 ± 3.9 Hz; SQ22, $n = 5$, 14.7 ± 7.1 Hz; 100 μM DDA, $n = 3$, 13.0 ± 7.9 Hz; 9-CPA, $n = 2$, 14.8 ± 3.4 Hz).

An effective inhibition of DA-elicited peripheral spike initiation by blockers of I_h was shown using intracellular recordings and application to the entire PD axon (Ballo and Bucher, 2009). We wanted to confirm these results and test the magnitude of the effect with the same focal axonal applications as used above. Figure 2*A* shows mean maximum spike frequencies measured in these experiments ($n = 5$). When DA was applied in conjunction with 5 mM CsCl, only a small increase in spike frequency was observed. After a 20–30 min wash, DA was applied alone and showed an increase in spike frequency comparable with the one shown in Figure 1*C*. The increase in spike frequency in DA alone was significant from the three preceding treatments, whereas there were no significant differences between control, DA plus CsCl, and wash (repeated-measures ANOVA, $p < 0.001$, Fisher's PLSD *post hoc* tests).

Even though these results argue that the DA effect is mostly mediated by I_h and therefore potentially directly by increased cAMP levels, we wanted to test whether indirect (phosphorylation-dependent) effects of increased cAMP levels may play a role. Therefore, we tested H89, which inhibits PKA activity in crayfish proprioceptor neurons and glia cells (Uzdensky et al., 2007). H89 alone had no effect on peripheral spiking ($n = 3$) but increased firing when applied in conjunction with DA. Figure 2*B* shows an experiment in which DA was applied alone first, and then, after spike frequency had decayed markedly from its peak value, in conjunction with H89. Figure 2*C* shows that, across experiments, H89 significantly increased spike frequency from 10.3 ± 0.9 to 14.0 ± 1.1 Hz ($n = 4$; paired t test, $p < 0.05$). Note that reapplication of DA alone does not have this effect (Fig. 1*B*). With the caveat that the specificity of H89 to PKA in this system is not known, the result suggests that there may be a PKA-mediated inhibitory effect on peripheral spike initiation, either counteracting direct cAMP effects on HCN channels or affecting other currents (e.g., increasing K^+ conductances).

Voltage-clamp recordings from the PD axon reveal the presence of I_h

The PD axons display a substantial depolarizing sag potential in response to hyperpolarizing current injection, and blockers of I_h inhibit peripheral spike initiation in response to DA application (Ballo and Bucher, 2009) (experiments described above). In addition, our results from pharmacological experiments are consistent with an increase in cAMP. Therefore, we wanted to test the effect of DA on I_h directly. To this end, we obtained two-electrode voltage-clamp recordings from the axon in the *dvn* (Fig. 3*A*). The length constant of the PD axon is ~1.5 mm (Ballo and Bucher, 2009). We routinely obtained good voltage control, probably aided by the fact that I_h is a slow current and no fast transients had to be clamped. Figure 3*B* shows the current response to a voltage step from −30 to −120 mV in control and 5 mM CsCl. CsCl blocked most of a slowly activating inward current that invariably did not reach steady state within the 15 s voltage steps used.

DA shifts the reversal potential of I_h in the depolarizing direction

I_h is a mixed cation current, as the underlying channels are permeable to Na^+ and K^+, generally thought to be at a fixed ratio that yields the specific reversal potential in a given case (Biel et al., 2009; Wahl-Schott and Biel, 2009). Nevertheless, we found that the reversal potential changed between control saline and DA application. We calculated the reversal potential from tail current measurements ($n = 4$). Figure 4*A* shows leak-subtracted tail cur-

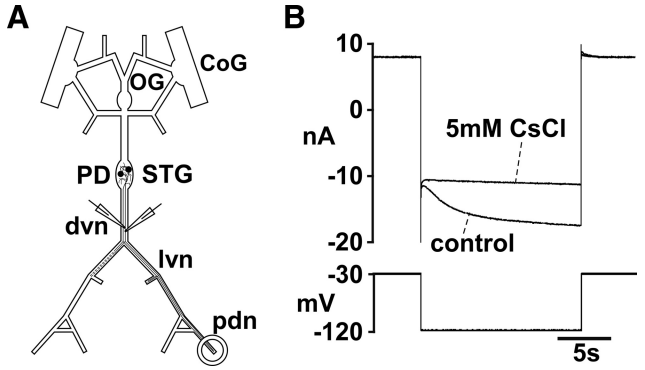

Figure 3. Two-electrode voltage-clamp measurement of I_h. ***A***, Schematic of the STNS and electrode positions. Channel blockers were bath applied. ***B***, Current response to a 15 s voltage step from −30 to −120 mV in the presence of TTX, TEA, and 4-AP. The slowly activating inward current is almost completely blocked by subsequent addition of CsCl.

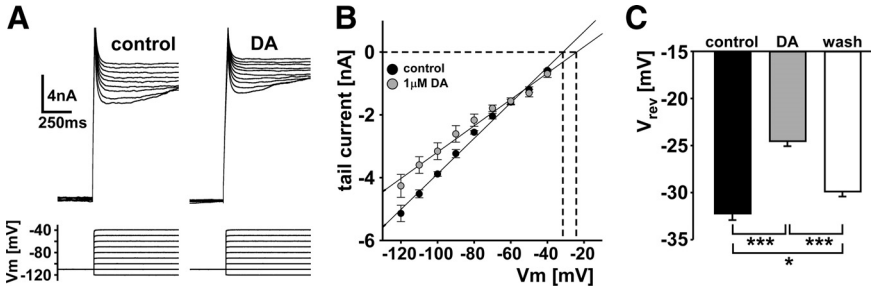

Figure 4. DA effect on tail currents and reversal potential. ***A***, Example leak-subtracted tail currents in control and DA. The membrane potential was stepped to −110 mV for 15 s and then to potentials between −120 and −40 mV for 4 s. ***B***, *I–V* plot from means of tail current measurements ($n = 4$). ***C***, Reversal potentials in control, DA, and wash, as determined from the zero crossings of individual *I–V* plots. Statistical differences were determined by repeated-measures ANOVA and Fisher's PLSD *post hoc* comparisons. *$p < 0.05$; ***$p < 0.001$. Error bars are SEM.

rents in control and DA, measured from a −110 mV prestep to test potentials between −120 and −40 mV. Figure 4*B* shows that linear fits to *I–V* plots of tail currents had different slopes and zero crossings between control and DA. The extrapolated reversal potential in DA was shifted in the depolarized direction, from −32.3 ± 0.6 to −24.6 ± 0.5 mV, and back to a more hyperpolarized value (29.9 ± 0.5 mV) after wash (Fig. 4*C*). These changes were significant (repeated-measures ANOVA, $p < 0.001$, Fisher's PLSD *post hoc* comparisons). Note that the reversal potential values are close to the holding potential of −30 mV, which explains the absence of substantial tail currents in the following experiments.

DA increases I_h at biologically relevant membrane potentials

The mean reversal potential values obtained from the four experiments described above were used to calculate conductance values from I_h measurements in seven experiments. Figure 5*A* shows voltage-clamp traces obtained in control saline and DA. These traces show no obvious change, possibly because they were not leak-subtracted, but we found significant changes in I_h activation between control and DA across experiments. Figure 5*B* shows activation curves of I_h in control saline, DA, and after 20 min of wash. DA reduced the maximum conductance significantly, but increased conductance at more depolarized membrane potentials. The asterisks in Figure 5*B* indicate statistical significance between control and DA determined by a two-way ANOVA ($p < 0.001$) and Fisher's PLSD *post hoc* tests. At potentials more negative than −80 mV, conductance was reduced, but between −70 and −50 mV (Fig. 5*B*, gray box) conductance was increased. The calculated maximal conductance decreased significantly from 67 ± 4 nS in control to 48 ± 3 nS in DA and did not return to control levels after wash but increased to 53 ± 4 nS (repeated-measures ANOVA, $p < 0.001$, Fisher's PLSD *post hoc* tests) (Fig. 5*E*).

The increase in conductance around normal resting membrane potentials in DA was attributable to a shift of the activation curve in the depolarizing direction and a change in slope, as can be seen more clearly when normalized conductances are plotted (Fig. 5*C*). The voltage of half-activation was significantly more depolarized in DA (−74 ± 2 mV) than in control (−82 ± 2 mV), an effect that washed completely (−83 ± 2 mV) (repeated-measures ANOVA, $p < 0.001$, Fisher PLSD *post hoc* tests) (Fig. 5*F*). In addition, the total range in which conductance was voltage dependent broadened (Fig. 5*C*), as indicated by a significant change in the slope factor from −8.5 ± 0.6 mV in control to −12.9 ± 1.5 mV in DA that also washed (−9.9 ± 0.6 mV) (Fig. 5*G*).

The changes in conductance at biologically relevant membrane potentials seem small when viewed in reference to the maximal conductance values. However, conductance in DA actually increased to ~150–300% of control values between −70 and −50 mV (Fig. 5*D*, gray box, black circles). The differences between control and DA are not the consequence of the altered reversal potential in DA. In fact, the depolarizing shift in the reversal potential as measured in DA leads to a reduction of the difference. The gray circles in Figure 5*D* show the increase when conductance in DA is calculated with the same reversal potential as in control, indicating that, if the change of the reversal potential is ignored, the effect of DA on conductance is even larger.

In contrast to the changes affecting steady-state conductances, the activation kinetics did not change. The activation time constants measured from the current response to a step from −30 to −110 mV in control (3.7 ± 0.2 s) and DA (3.8 ± 0.2 s) were not significantly different (paired *t* test, $p = 0.914$).

Observed changes in I_h activation are not attributable to DA effects on other currents

The experiments described above were done in the presence of TTX, 4-AP, and TEA. We previously found no evidence for the presence of axonal Ca^{2+} currents or Ca^{2+}-activated K^+ currents (Ballo and Bucher, 2009) (A. W. Ballo, unpublished observations). In addition, the unusual voltage range of I_h activation makes it unlikely that other previously unidentified currents directly contaminated our measurements, particularly at more hyperpolarized potentials. However, we wanted to ensure that the changes we observed in DA were solely attributable to modulation of I_h. To this end, in three experiments we added 5 mM CsCl to the mixture of blockers and used the same voltage-clamp protocol as for I_h measurements, first without and then in the presence of DA. Figure 6*A* shows overlaid current traces obtained in the presence of CsCl (black) and in the presence of CsCl plus DA

(gray). Neither the holding current nor the step responses showed substantial differences. Figure 6*B* shows the *I–V* plots from mean values of the three experiments. Current values were obtained from the end of the steps and were virtually indistinguishable between CsCl alone and CsCl plus DA. We are therefore confident that the observed changes in I_h activation are not contaminated by effects of DA on other currents.

Changes in I_h activation are not caused by "rundown"

Because the reduction of maximal conductance in DA did not wash completely, we wanted to test whether this effect was attributable to rundown rather than to a specific effect of DA signaling. Such rundown of I_h has been observed in other systems and has been proposed to be attributable to changing basal cAMP levels during the experimental time course (DiFrancesco et al., 1986; Chen et al., 2001). Therefore, we repeated the I_h measurement in four experiments in control saline with the same experimental time course as we used in the DA experiments (i.e., with a 20 min interval between voltage-clamp protocols). Figure 7*A* shows that repeatedly measuring I_h did not change the activation curve.

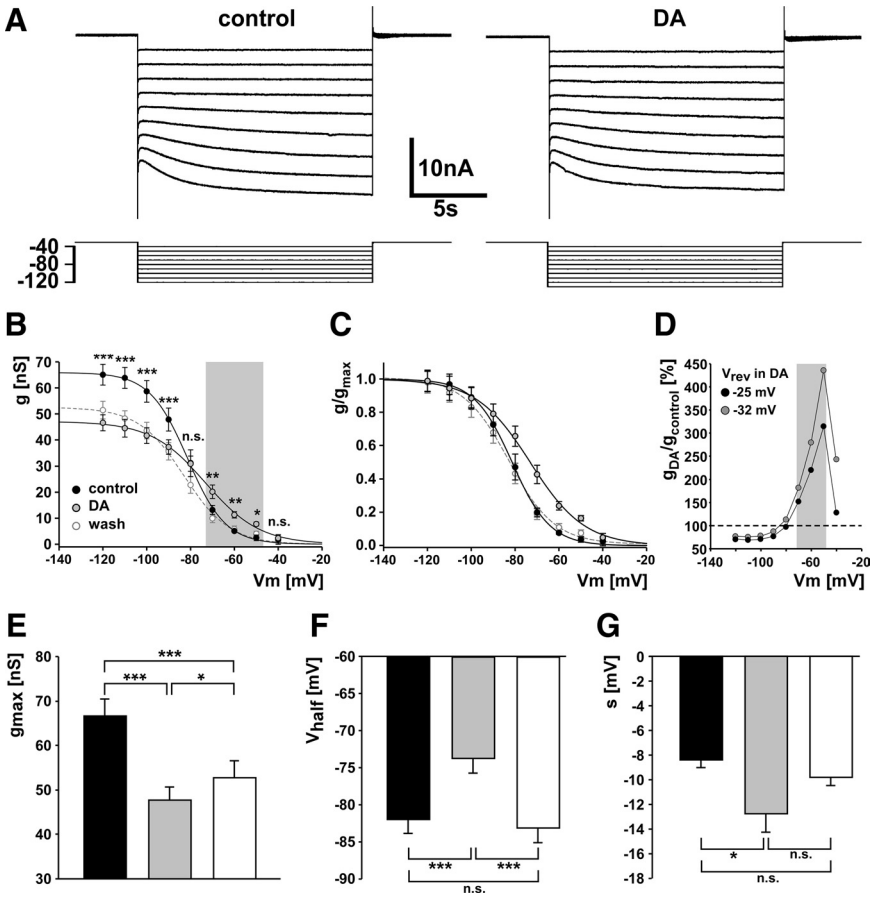

Figure 5. DA modulation of I_h activation. ***A***, Current measurements in control and DA, obtained from stepping from a holding potential of −30 mV to potentials between −40 and −120 mV for 15 s. ***B***, Activation curves for I_h conductances in control, DA, and wash. Statistical differences between treatments at given step voltages were determined using two-way ANOVA and Fisher's PLSD *post hoc* comparisons. The gray shading indicates "biologically relevant" potentials. ***C***, Activation curves from conductance measurements normalized to the maximal conductances. ***D***, Percentage difference of conductances (DA/control). The gray shading indicates biologically relevant potentials. Conductances in DA were calculated both with the mean reversal potential measured in DA, and with the same reversal potential as in control. ***E–G***, Maximal conductances, voltage of half-activation, and slope factor values determined from first-order Boltzman fits to the individual plots of conductance over voltage. Statistical significance was determined by repeated-measures ANOVA and Fisher's PLSD *post hoc* comparisons. $*p < 0.05$; $**p < 0.01$; $***p < 0.001$. Error bars are SEM.

Changes in I_h activation are attributable to increased cAMP levels but not dependent on PKA

The reduction of maximal conductance paired with a depolarizing shift of the activation curve and an increase in the voltage-dependent range are unusual, and the fact that changes in maximal conductance and voltage dependence are differentially affected during washing raises the question of whether they represent separate mechanisms. Potentially, these changes may not be mediated through the cyclic nucleotide binding domain of the channels. For example, signaling pathways independent of cAMP (Biel et al., 2009; Wahl-Schott and Biel, 2009), as well as PKA-dependent pathways mediating phosphorylation-dependent effects (Chang et al., 1991; Vargas and Lucero, 2002), could play a role. We therefore wanted to test the dependence both on cAMP and on PKA. Because all drugs that elicited peripheral spike initiation did so at lower frequency than DA (Fig. 1*C*), we used a combination of 30 μM IBMX and 10 μM forskolin to ensure a substantial increase in cAMP concentration. We measured I_h in control saline and in IBMX plus forskolin in three experiments. Figure 7*B* shows that increased cAMP levels have similar effects as application of DA. The maximal conductance is decreased while the activation curve is shifted in the depolarizing direction, so that conductance around biologically relevant membrane potentials is increased. In addition, these changes appear to be independent of PKA signaling. In three experiments, we measured I_h in control saline and then applied 20 μM H89 for 20 min. Subsequently, I_h was measured in H89 plus DA. Figure 7*C* shows that H89 neither blocks the reduction in maximal conductance nor the change in voltage dependence elicited by DA.

The changes in activation properties are not qualitatively affected by space-clamp errors

Space-clamp errors can significantly distort activation curves measured in neuronal compartments that are not electrotonically compact (Bar-Yehuda and Korngreen, 2008). Therefore, we wanted to make sure that the changes in maximal conductance and voltage dependence are not qualitatively affected by limited spatial control during voltage-clamp recordings. To this end, a multicompartmental mathematical model of the axon was used to simulate effects of space-clamp errors. The basic approach was to "reverse engineer" the actual I_h activation parameters that yield the measured experimental values. In two-electrode voltage-clamp experiments, the space-clamp error does not just depend on the cable properties of the axon but also on the distance between injecting and measuring electrodes. In our experiments, electrodes were placed at distances between 0 and 1 mm, usually at ~0.5 mm. We simulated voltage-clamp experiments with varying electrode distances. Figure 8*A* shows Boltzman plots

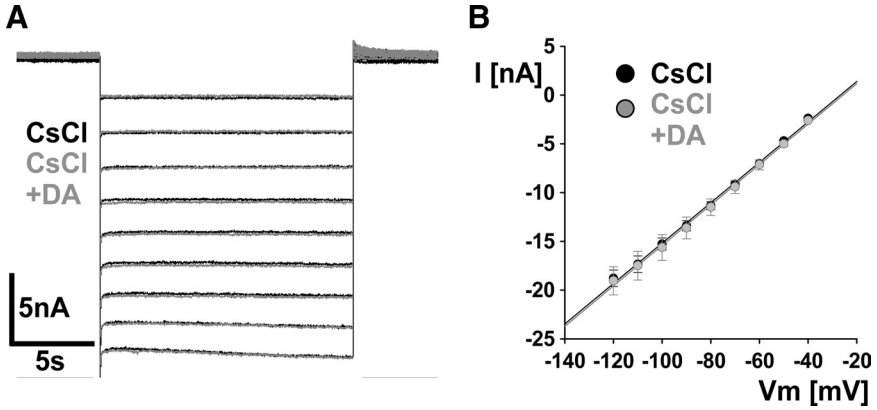

Figure 6. Observed changes in I_h activation were not attributable to DA effects on other currents. ***A***, Overlaid current responses to the same voltage step protocol used for I_h measurements, in the presence of CsCl (black), and in the presence of CsCl plus DA (gray). ***B***, *I–V* plot of mean values from three experiments, obtained from the end of the steps. Error bars are SEM.

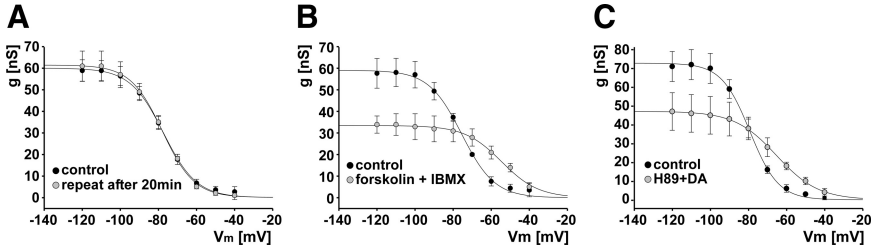

Figure 7. Observed changes in I_h activation were attributable to PKA-independent effects of cAMP. ***A***, Activation curves for I_h measured repeatedly in the absence of DA, but with the same experimental time course ($n = 4$). ***B***, I_h activation curves in control and in the presence of forskolin and IBMX ($n = 3$). ***C***, I_h activation curves in control and in H89 plus DA ($n = 3$). Error bars are SEM.

of the experimental values from Figure 5, but here normalized to the maximal conductance in control. Figure 8*B* shows the reconstructed activation curves from a simulated two-electrode voltage-clamp experiment with a distance of 0.5 mm between injection and measurement electrodes. The maximal specific membrane conductances (conductance/membrane area) in control and DA were normalized to the control value. Even though activation is steeper and at more depolarized potentials, the differences between control and DA are qualitatively the same. Maximal conductance is reduced to 62% of control in DA (compared with 73% in the experimental data), the voltage of half-activation changes in the depolarizing direction from −80 mV in control to −72.5 mV in DA (compared with −82.0 and −73.8 mV in the experimental data), and the slope is shallower in DA (with the slope factor changing from 5.5 to 9.2 mV, compared with 8.5 and 12.9 mV in the experimental data). Note that the parameter values reported above for the model are values actually put into the model; these values produce a good match between the voltage-clamp measurements in the model and the experimental measurements both in control and in DA. Most importantly, conductance at biologically relevant membrane potentials is increased despite the reduction in maximal conductance (Fig. 8*A*,*B*, shaded areas). We are therefore confident that our experimental findings regarding the effect of DA on the steady-state activation properties of I_h are not qualitatively affected by space-clamp errors.

Because the goal of this model was to see whether the effect of DA on I_h is affected by space-clamp measurements, we used the model to find out the extent to which the distance between the recording and measurement electrodes changed the measured DA effects. Figure 8*C–E* shows how, in the model, the distance between the two electrodes affects the measured DA effects on maximal conductance, voltage of half-activation, and the slope factor, respectively. As in the experimental data obtained at an electrode distance of ~0.5 mm, in the range of 0.0–1.9 mm the maximal conductance is always reduced in DA (Fig. 8*C*), the voltage of half-activation is always shifted in the depolarizing direction (Fig. 8*D*), and the slope factor is shifted in the negative direction (Fig. 8*E*). Therefore, the steady-state activation properties of I_h would not be qualitatively affected by space-clamp errors even at electrode distances greater than in our experiments.

Discussion

We show here that, in the PD axons of *H. americanus*, depolarization and peripheral spike initiation elicited by DA are likely caused by a D_1-type receptor mechanism increasing cAMP levels. The predominant effect of increased cAMP concentration is a modulation of I_h, resulting in an increase of conductance at biologically relevant membrane potentials.

Dopaminergic signaling in the PD axons

In the STNS of decapods, DA effects are mostly mediated by different types of G-proteins (Clark et al., 2008). Although D_2-type receptors can couple through multiple types of G-proteins, some of which can increase cAMP levels in a heterologous expression system (Clark and Baro, 2007), increased cAMP levels are predominantly attributable to D_1-type receptors in the native tissue (Clark et al., 2008). We show that the DA effect on the PD axons is consistent with an increase in cAMP. Application of D_1-type receptor agonists as well as pharmacological activation of AC and inhibition of PDE mimicked peripheral spike initiation as seen in response to DA.

We did not see effects of inhibitors of AC, and cAMP analogs alone did not elicit peripheral spikes. AC blockers have been used successfully in crustacean olfactory neurons (Doolin and Ache, 2005), but the pharmacological profile of AC in the PD axons may be different. The small effect of cAMP analogs may be attributable to insufficient access to the axonal cytosol in whole-nerve tissue, or to poor access to compartmentalized G-protein-coupled receptor signaling protein complexes (Hall and Lefkowitz, 2002; Rebois and Hébert, 2003).

We can neither exclude the possibility that additional types of DA receptors are expressed in the PD axons, nor that additional signaling mechanisms, other than activation of stimulating G-proteins, play a role. However, our results are consistent with a DA-mediated increase in cAMP levels, which suggests a D_1-type receptor mechanism.

Interestingly, the PD neurons in the spiny lobster *Panulirus interruptus* only express D_2-type receptors in the STG neuropil (Oginsky et al., 2010), and I_h is not modulated by DA when measured from the soma (Peck et al., 2006). Our results may either point to differences in receptors and signaling pathways between cell compartments or to a difference between species.

Activation properties of I_h in the PD axon

I_h shows similar characteristics between vertebrates and invertebrates. In vertebrates, four genes code for pore-forming subunits (HCN1–4), which form different homotetramers or heterotetramers with distinct properties (Robinson and Siegelbaum, 2003; Biel et al., 2009; Wahl-Schott and Biel, 2009). In crustaceans, as in other invertebrates, extensive splicing of a single gene gives rise to multiple potential transcripts of HCN homologs (Gisselmann et al., 2005; Ouyang et al., 2007). Despite similar voltage dependence and pharmacology, channel activation in crustaceans is substantially slower than in vertebrates. Our measurements of I_h in the PD axons show maximal conductance values, voltage dependence, and activation kinetics that are within the range of those in central compartments of stomatogastric neurons (Golowasch and Marder, 1992; Kiehn and Harris-Warrick, 1992; Harris-Warrick et al., 1995; Peck et al., 2006; Ouyang et al., 2007).

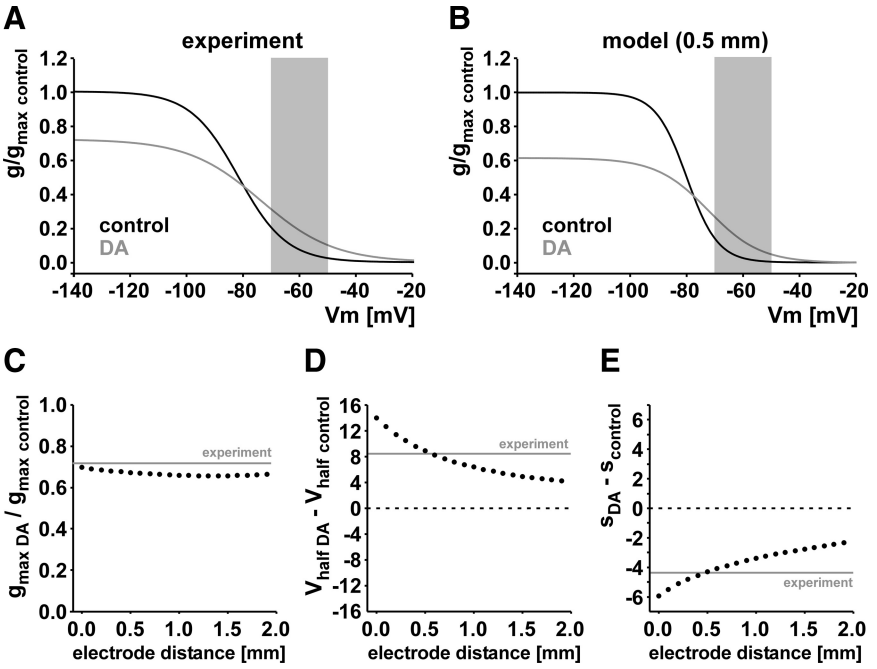

Figure 8. The experimentally observed reduction of maximal conductance and increase of conductance at biologically relevant membrane potentials (shaded areas) are not qualitatively different when space-clamp errors are considered. ***A***, I_h activation curves plotted as Boltzman equations from the experimentally obtained mean values shown in Figure 5 for control and DA, normalized to the maximal conductance in control. ***B***, Reverse-engineered activation curves from a simulated two-electrode voltage-clamp experiment with an electrode distance of 0.5 mm. These activation properties gave rise to values very similar to the ones experimentally observed. ***C***, Maximal conductance in DA as a fraction of the control value in axon models with different assumed electrode distances from 0 to 1.9 mm. All measurements showed reduced maximal conductances similar to the experimentally obtained value (gray line). ***D***, The shift in the voltage of half-activation between control and DA, obtained from the same model measurements as in ***C***. In all cases, the shift is in the depolarizing direction. ***E***, The change in slope factor between control and DA as a function of electrode distance. In all cases, the slope factor changes becomes more negative, leading to shallower activation curves in DA and therefore to an increased range over which activation is voltage dependent.

Dopamine modulation of I_h

DA receptor pathways commonly affect cAMP production (Gingrich and Caron, 1993; Neve et al., 2004). Because of the fact that HCN-type channels have a cyclic-nucleotide binding domain (Robinson and Siegelbaum, 2003; Biel et al., 2009; Wahl-Schott and Biel, 2009), I_h is a fairly common target of DA modulation (Jiang et al., 1993; Wu and Hablitz, 2005; Peck et al., 2006; Chen and Yang, 2007; Deng et al., 2007). In the STG, DA modulates many voltage-gated conductances in a cell type-specific manner, including I_h (Harris-Warrick et al., 1998; Kloppenburg et al., 1999, 2000; Peck et al., 2001, 2006; Johnson et al., 2003; Gruhn et al., 2005). In voltage-clamp recordings of I_h from somata of a subset of STG neurons in *P. interruptus*, DA both shifts the activation curve and increases maximal conductance (Peck et al., 2006). In contrast, we found a decrease in maximal conductance in the PD axons, accompanied by a shift in activation curve and change in slope. The changes in the voltage dependence were sufficient to increase conductance at biologically relevant potentials, despite the decrease in maximal conductance. We show that this decrease was neither attributable to other currents nor to rundown, and similar changes in maximal conductance and voltage dependence were observed when cAMP levels were raised pharmacologically. With the caveat that the specificity of H89 in this system is not well known, DA modulation of I_h did not appear to depend on PKA, as it is in the mammalian heart and in rat olfactory neurons (Chang et al., 1991; Vargas and Lucero, 2002). The positive effect of H89 on spike initiation (Fig. 2*B*,*C*) could be attributable to modulation of other ionic conductances.

We also excluded the possibility that the effects of DA on I_h activation were qualitatively changed by limited spatial control during our voltage-clamp experiments. Space-clamp errors can substantially distort activation curve measurements (Bar-Yehuda and Korngreen, 2008), and a change in I_h should change the specific membrane resistance and therefore the length constant of the axon. However, we show in a computational model that both the change in maximal conductance and the changes in voltage dependence are qualitatively similar with or without correction for space-clamp errors.

Another surprising result was the DA-induced change in reversal potential. Permeability of HCN channels for Na^+ and K^+ are not independent, and Na^+ permeability is dependent on the extracellular K^+ concentration (Ludwig et al., 1998). We can only speculate whether such a change in K^+ concentration could occur at the PD axons, for example because of a DA effect on surrounding glia cells. However, the observed changes in activation properties are not attributable to the change in reversal potential, as such a change reduces the difference in conductance between control and DA at biologically relevant potentials (Fig. 5*D*).

Functional implications of the presence and DA modulation of I_h in the PD axons

I_h is commonly found in nonsynaptic axonal membrane, both in peripheral and central neurons (Nashmi and Fehlings, 2001; Krishnan et al., 2009; Nusser, 2009). One possible function of axonal I_h is to balance activity-dependent hyperpolarization caused by activation of K^+ currents or the Na^+/K^+ pump to improve the conduction reliability during repetitive spiking (Grafe et al., 1997; Soleng et al., 2003; Kiernan et al., 2004; Baginskas et al., 2009).

The PD axons display poor temporal fidelity in control saline, as conduction velocity during normal rhythmic motor activity

changes substantially over the course of single bursts (Ballo and Bucher, 2009). Inward rectification through I_h potentially plays an important role in balancing a slow afterhyperpolarization, and this "tug-of-war" renders the axonal interburst membrane potential dependent on the strength of ongoing activity (Ballo and Bucher, 2009). Because of slow afterhyperpolarization, the membrane potential between bursts is the more hyperpolarized the stronger the bursting activity is. Enhancement of I_h by DA causes increased inward rectification and therefore less hyperpolarization. Because spike conduction velocity should depend on the resting membrane potential, I_h in the PD axons may be crucial for controlling temporal fidelity of axonal spike conduction, and DA modulation of I_h may have a substantial effect on this fidelity.

How common is neuromodulation of axon trunks?

There still is a dearth of information about the specific spatial distribution of receptors and ion channels in neurons (Trimmer and Rhodes, 2004; Nusser, 2009), and physiological recordings from axons in many neuron types are difficult with conventional methods (Debanne, 2004). That said, there are examples for axonal neuromodulation from both invertebrate and vertebrate preparations. Acetylcholine controls axonal excitability in the thalamocortical pathway (Kawai et al., 2007), induces Ca^{2+} influx in optic nerve axons (Zhang et al., 2004), and does both in unmyelinated peripheral C-fibers (Lang et al., 2003). GABA blocks spike conduction in some mammalian sensory axons (Verdier et al., 2003), inhibits Ca^{2+} transients in developing optic nerve (Sun and Chiu, 1999), and causes changes in spike conduction in spinal and optic nerve axons (Sakatani et al., 1991, 1993). Serotonin modulates excitability in unmyelinated peripheral nerve fibers (Lang et al., 2006) and controls conduction block in leech sensory neurons (Mar and Drapeau, 1996; Scuri et al., 2007).

Several examples come from the STNS of crabs, with demonstrated physiological functions. Octopamine elicits spiking in the axon of a descending projection neuron, centimeters from central neuropil (Goaillard et al., 2004). It also activates the axon of a proprioceptive neuron at an additional spike initiation site distant from the muscle–tendon organ it innervates (Daur et al., 2009). In both cases, additional spiking generated in the axon affects pattern generation in the target circuits. In a stomatogastric motor axon, centrally generated bursts trigger sustained peripheral spike initiation in the presence of serotonin, which prolongs contraction in a subset of target muscles (Meyrand et al., 1992). These examples and our results argue that axon trunks do not just faithfully conduct spikes but can play an important role in shaping neuronal output.

References

Baginskas A, Palani D, Chiu K, Raastad M (2009) The H-current secures action potential transmission at high frequencies in rat cerebellar parallel fibers. Eur J Neurosci 29:87–96.

Ballo AW, Bucher D (2009) Complex intrinsic membrane properties and dopamine shape spiking activity in a motor axon. J Neurosci 29:5062–5074.

Bar-Yehuda D, Korngreen A (2008) Space-clamp problems when voltage clamping neurons expressing voltage-gated conductances. J Neurophysiol 99:1127–1136.

Bean BP (2007) The action potential in mammalian central neurons. Nat Rev Neurosci 8:451–465.

Biel M, Wahl-Schott C, Michalakis S, Zong X (2009) Hyperpolarization-activated cation channels: from genes to function. Physiol Rev 89:847–885.

Bucher D, Thirumalai V, Marder E (2003) Axonal dopamine receptors activate peripheral spike initiation in a stomatogastric motor neuron. J Neurosci 23:6866–6875.

Butt SJ, Pitman RM (2002) Modulation by 5-hydroxytryptamine of nicotinic acetylcholine responses recorded from an identified cockroach (*Periplaneta americana*) motoneuron. Eur J Neurosci 15:429–438.

Chang F, Cohen IS, DiFrancesco D, Rosen MR, Tromba C (1991) Effects of protein kinase inhibitors on canine Purkinje fibre pacemaker depolarization and the pacemaker current I_f. J Physiol 440:367–384.

Chen L, Yang XL (2007) Hyperpolarization-activated cation current is involved in modulation of the excitability of rat retinal ganglion cells by dopamine. Neuroscience 150:299–308.

Chen S, Wang J, Siegelbaum SA (2001) Properties of hyperpolarization-activated pacemaker current defined by coassembly of HCN1 and HCN2 subunits and basal modulation by cyclic nucleotide. J Gen Physiol 117:491–504.

Clark MC, Baro DJ (2007) Arthropod D_2 receptors positively couple with cAMP through the Gi/o protein family. Comp Biochem Physiol B Biochem Mol Biol 146:9–19.

Clark MC, Khan R, Baro DJ (2008) Crustacean dopamine receptors: localization and G protein coupling in the stomatogastric ganglion. J Neurochem 104:1006–1019.

Clemens S, Calin-Jageman R, Sakurai A, Katz PS (2007) Altering cAMP levels within a central pattern generator modifies or disrupts rhythmic motor output. J Comp Physiol A Neuroethol Sens Neural Behav Physiol 193:1265–1271.

Daur N, Nadim F, Stein W (2009) Regulation of motor patterns by the central spike-initiation zone of a sensory neuron. Eur J Neurosci 30:808–822.

Debanne D (2004) Information processing in the axon. Nat Rev Neurosci 5:304–316.

Debanne D, Guérineau NC, Gähwiler BH, Thompson SM (1997) Action-potential propagation gated by an axonal I_A-like K^+ conductance in hippocampus. Nature 389:286–289.

Debanne D, Kopysova IL, Bras H, Ferrand N (1999) Gating of action potential propagation by an axonal A-like potassium conductance in the hippocampus: a new type of non-synaptic plasticity. J Physiol Paris 93:285–296.

De Col R, Messlinger K, Carr RW (2008) Conduction velocity is regulated by sodium channel inactivation in unmyelinated axons innervating the rat cranial meninges. J Physiol 586:1089–1103.

Deng P, Zhang Y, Xu ZC (2007) Involvement of I_h in dopamine modulation of tonic firing in striatal cholinergic interneurons. J Neurosci 27:3148–3156.

DiFrancesco D, Ferroni A, Mazzanti M, Tromba C (1986) Properties of the hyperpolarizing-activated current (if) in cells isolated from the rabbit sino-atrial node. J Physiol 377:61–88.

Doolin RE, Ache BW (2005) Cyclic nucleotide signaling mediates an odorant-suppressible chloride conductance in lobster olfactory receptor neurons. Chem Senses 30:127–135.

Genovese G, Senek M, Ortiz N, Regueira M, Towle DW, Tresguerres M, Luquet CM (2006) Dopaminergic regulation of ion transport in gills of the euryhaline semiterrestrial crab *Chasmagnathus granulatus*: interaction between D_1- and D_2-like receptors. J Exp Biol 209:2785–2793.

Gingrich JA, Caron MG (1993) Recent advances in the molecular biology of dopamine receptors. Annu Rev Neurosci 16:299–321.

Gisselmann G, Marx T, Bobkov Y, Wetzel CH, Neuhaus EM, Ache BW, Hatt H (2005) Molecular and functional characterization of an I_h-channel from lobster olfactory receptor neurons. Eur J Neurosci 21:1635–1647.

Goaillard JM, Schulz DJ, Kilman VL, Marder E (2004) Octopamine modulates the axons of modulatory projection neurons. J Neurosci 24:7063–7073.

Golowasch J, Marder E (1992) Ionic currents of the lateral pyloric neuron of the stomatogastric ganglion of the crab. J Neurophysiol 67:318–331.

Goy MF, Kravitz EA (1989) Cyclic AMP only partially mediates the actions of serotonin at lobster neuromuscular junctions. J Neurosci 9:369–379.

Grafe P, Quasthoff S, Grosskreutz J, Alzheimer C (1997) Function of the hyperpolarization-activated inward rectification in nonmyelinated peripheral rat and human axons. J Neurophysiol 77:421–426.

Gruhn M, Guckenheimer J, Land B, Harris-Warrick RM (2005) Dopamine modulation of two delayed rectifier potassium currents in a small neural network. J Neurophysiol 94:2888–2900.

Hall RA, Lefkowitz RJ (2002) Regulation of G protein-coupled receptor signaling by scaffold proteins. Circ Res 91:672–680.

Harris-Warrick RM, Coniglio LM, Levini RM, Gueron S, Guckenheimer J (1995) Dopamine modulation of two subthreshold currents produces phase shifts in activity of an identified motoneuron. J Neurophysiol 74:1404–1420.

Harris-Warrick RM, Johnson BR, Peck JH, Kloppenburg P, Ayali A, Skarbinski J (1998) Distributed effects of dopamine modulation in the crustacean pyloric network. Ann N Y Acad Sci 860:155–167.

Jiang YQ, Xing GG, Wang SL, Tu HY, Chi YN, Li J, Liu FY, Han JS, Wan Y (2008) Axonal accumulation of hyperpolarization-activated cyclic nucleotide-gated cation channels contributes to mechanical allodynia after peripheral nerve injury in rat. Pain 137:495–506.

Jiang ZG, Pessia M, North RA (1993) Dopamine and baclofen inhibit the hyperpolarization-activated cation current in rat ventral tegmental neurones. J Physiol 462:753–764.

Johnson BR, Kloppenburg P, Harris-Warrick RM (2003) Dopamine modulation of calcium currents in pyloric neurons of the lobster stomatogastric ganglion. J Neurophysiol 90:631–643.

Kawai H, Lazar R, Metherate R (2007) Nicotinic control of axon excitability regulates thalamocortical transmission. Nat Neurosci 10:1168–1175.

Kepler TB, Marder E (1993) Spike initiation and propagation on axons with slow inward currents. Biol Cybern 68:209–214.

Kiehn O, Harris-Warrick RM (1992) 5-HT modulation of hyperpolarization-activated inward current and calcium-dependent outward current in a crustacean motor neuron. J Neurophysiol 68:496–508.

Kiernan MC, Lin CS, Burke D (2004) Differences in activity-dependent hyperpolarization in human sensory and motor axons. J Physiol 558:341–349.

Kloppenburg P, Levini RM, Harris-Warrick RM (1999) Dopamine modulates two potassium currents and inhibits the intrinsic firing properties of an identified motor neuron in a central pattern generator network. J Neurophysiol 81:29–38.

Kloppenburg P, Zipfel WR, Webb WW, Harris-Warrick RM (2000) Highly localized Ca^{2+} accumulation revealed by multiphoton microscopy in an identified motoneuron and its modulation by dopamine. J Neurosci 20:2523–2533.

Kress GJ, Mennerick S (2009) Action potential initiation and propagation: upstream influences on neurotransmission. Neuroscience 158:211–222.

Krishnan AV, Lin CS, Park SB, Kiernan MC (2009) Axonal ion channels from bench to bedside: a translational neuroscience perspective. Prog Neurobiol 89:288–313.

Lang PM, Burgstahler R, Sippel W, Irnich D, Schlotter-Weigel B, Grafe P (2003) Characterization of neuronal nicotinic acetylcholine receptors in the membrane of unmyelinated human C-fiber axons by in vitro studies. J Neurophysiol 90:3295–3303.

Lang PM, Moalem-Taylor G, Tracey D, Bostock H, Grafe P (2006) Activity-dependent modulation of axonal excitability in unmyelinated peripheral rat nerve fibers by the 5-HT3 serotonin receptor. J Neurophysiol 96:2963–2971.

Ludwig A, Zong X, Jeglitsch M, Hofmann F, Biel M (1998) A family of hyperpolarization-activated mammalian cation channels. Nature 393:587–591.

Ma C, LaMotte RH (2007) Multiple sites for generation of ectopic spontaneous activity in neurons of the chronically compressed dorsal root ganglion. J Neurosci 27:14059–14068.

Mar A, Drapeau P (1996) Modulation of conduction block in leech mechanosensory neurons. J Neurosci 16:4335–4343.

Meeks JP, Mennerick S (2007) Action potential initiation and propagation in CA3 pyramidal axons. J Neurophysiol 97:3460–3472.

Meeks JP, Jiang X, Mennerick S (2005) Action potential fidelity during normal and epileptiform activity in paired soma-axon recordings from rat hippocampus. J Physiol 566:425–441.

Meyrand P, Weimann JM, Marder E (1992) Multiple axonal spike initiation zones in a motor neuron: serotonin activation. J Neurosci 12:2803–2812.

Miller RN, Rinzel J (1981) The dependence of impulse propagation speed on firing frequency, dispersion, for the Hodgkin-Huxley model. Biophys J 34:227–259.

Nashmi R, Fehlings MG (2001) Mechanisms of axonal dysfunction after spinal cord injury: with an emphasis on the role of voltage-gated potassium channels. Brain Res Brain Res Rev 38:165–191.

Neve KA, Seamans JK, Trantham-Davidson H (2004) Dopamine receptor signaling. J Recept Signal Transduct Res 24:165–205.

Nusser Z (2009) Variability in the subcellular distribution of ion channels increases neuronal diversity. Trends Neurosci 32:267–274.

Oginsky MF, Rodgers EW, Clark MC, Simmons R, Krenz WD, Baro DJ (2010) D_2 receptors receive paracrine neurotransmission and are consistently targeted to a subset of synaptic structures in an identified neuron of the crustacean stomatogastric nervous system. J Comp Neurol 518:255–276.

Ouyang Q, Goeritz M, Harris-Warrick RM (2007) *Panulirus interruptus* I_h-channel gene PIIH: modification of channel properties by alternative splicing and role in rhythmic activity. J Neurophysiol 97:3880–3892.

Peck JH, Nakanishi ST, Yaple R, Harris-Warrick RM (2001) Amine modulation of the transient potassium current in identified cells of the lobster stomatogastric ganglion. J Neurophysiol 86:2957–2965.

Peck JH, Gaier E, Stevens E, Repicky S, Harris-Warrick RM (2006) Amine modulation of I_h in a small neural network. J Neurophysiol 96:2931–2940.

Rebois RV, Hébert TE (2003) Protein complexes involved in heptahelical receptor-mediated signal transduction. Receptors Channels 9:169–194.

Robinson RB, Siegelbaum SA (2003) Hyperpolarization-activated cation currents: from molecules to physiological function. Annu Rev Physiol 65:453–480.

Sakatani K, Hassan AZ, Ching W (1991) Age-dependent extrasynaptic modulation of axonal conduction by exogenous and endogenous GABA in the rat optic nerve. Exp Neurol 114:307–314.

Sakatani K, Chesler M, Hassan AZ, Lee M, Young W (1993) Non-synaptic modulation of dorsal column conduction by endogenous GABA in neonatal rat spinal cord. Brain Res 622:43–50.

Scuri R, Lombardo P, Cataldo E, Ristori C, Brunelli M (2007) Inhibition of Na^+/K^+ ATPase potentiates synaptic transmission in tactile sensory neurons of the leech. Eur J Neurosci 25:159–167.

Soleng AF, Chiu K, Raastad M (2003) Unmyelinated axons in the rat hippocampus hyperpolarize and activate an H current when spike frequency exceeds 1 Hz. J Physiol 552:459–470.

Sun BB, Chiu SY (1999) N-type calcium channels and their regulation by GABAB receptors in axons of neonatal rat optic nerve. J Neurosci 19:5185–5194.

Trimmer JS, Rhodes KJ (2004) Localization of voltage-gated ion channels in mammalian brain. Annu Rev Physiol 66:477–519.

Uzdensky A, Lobanov A, Bibov M, Petin Y (2007) Involvement of Ca^{2+}- and cyclic adenosine monophosphate-mediated signaling pathways in photodynamic injury of isolated crayfish neuron and satellite glial cells. J Neurosci Res 85:860–870.

Vargas G, Lucero MT (2002) Modulation by PKA of the hyperpolarization-activated current (I_h) in cultured rat olfactory receptor neurons. J Membr Biol 188:115–125.

Verdier D, Lund JP, Kolta A (2003) GABAergic control of action potential propagation along axonal branches of mammalian sensory neurons. J Neurosci 23:2002–2007.

Wahl-Schott C, Biel M (2009) HCN channels: structure, cellular regulation and physiological function. Cell Mol Life Sci 66:470–494.

Wu J, Hablitz JJ (2005) Cooperative activation of D_1 and D_2 dopamine receptors enhances a hyperpolarization-activated inward current in layer I interneurons. J Neurosci 25:6322–6328.

Zhang CL, Verbny Y, Malek SA, Stys PK, Chiu SY (2004) Nicotinic acetylcholine receptors in mouse and rat optic nerves. J Neurophysiol 91:1025–1035.